Phase Transition Diagram for Underlay Heterogeneous Cognitive Radio Networks

Weng Chon Ao, Shin-Ming Cheng, and Kwang-Cheng Chen
Graduate Institute of Communication Engineering, National Taiwan University, Taipei 106, Taiwan
Email: r97942044@ntu.edu.tw, {smcheng, chenkc}@cc.ee.ntu.edu.tw

***Abstract*—Characterizing the topology and therefore fundamental limits is a must to establish effective end-to-end cognitive radio networking (CRN). However, there lacks complete understanding of the relationship among connectivity, interference, latency and other system parameters of the CRN. To clarify this complication, by employing tools from both percolation theory and stochastic geometry, we thus provide a novel parametrization of underlay secondary ad hoc CRN wherein the secondary network is regarded as an operating point in the *phase space*. Coexisting with a primary ad hoc network, the secondary network undergoes a *phase transition* due to avoiding interference to primary receivers, while being interfered by primary transmitters. Furthermore, transmit power allocation of secondary users is represented by a Pareto contour in the *phase space*, and the impact of interference on connectivity is captured by the *latency-to-percolate*. Finally, with the cognitive capability of CR, performance improvement of importing an SU-avoidance region around primary receivers is analyzed, and CRNs can be therefore successfully supplied.**

I. Introduction

Cognitive radio (CR) has emerged as a promising technology to enhance spectrum utilization by sensing the spectrum and opportunistic accessing the spectrum of primary (licensed) systems. The cognitive principle states that secondary (unlicensed) users (SUs/CRs) are aware of avoiding harmful interference with primary users (PUs); however, since SUs are transparent to PUs, the signal reception of an SU is exposed to interference from PUs. In other words, the density of active secondary transmitters (STs) should be limited to maintain the outage constraints of primary receivers (PRs), while the maximum transmission distance between a secondary receiver (SR) and an ST with fixed transmit power, for signal reception meeting the outage constraints of SRs, is reduced due to interference from active primary transmitters (PTs). Inspired by percolation theory, we parametrize the secondary network composed of SUs by a tuple (λ_{SU}, r_{SU}). It is regarded as an operating point in the phase space defined as (λ, r) as shown in Fig 1, where λ represents the density of active nodes and r represents the transmission range of a node, which is defined based on an outage constraint. When coexisting with the primary network composed of PUs, the topology change of the underlay secondary network is captured by the movement of its operating point in the phase space. The application of percolation theory in analyzing the impact of interference on connectivity in homogeneous wireless ad hoc network was discussed in [1], [2]. We generalize the idea to heterogeneous environment where a primary ad hoc network and a secondary ad hoc cognitive radio network (CRN) coexists.

To obtain the operating end point in the phase space, we adopt results from stochastic geometry, specifically Poisson point process, characterizing the aggregate interference from spatial point processes under different channel models. Some related works using similar techniques include topics on transmission capacity in wireless ad hoc network, defined as the product of the density of successful transmissions and the data rate with an outage constraint, which was introduced in [3]–[5]. Research recently developed along the lines of transmission capacity includes spectrum sharing in two-tier femtocell networks [6], [7], coexistence between cellular network and ad hoc network [8], and overlaid ad hoc network [9]. Earlier characterization of connectivity region of the CRN under protocol model does not account for aggregate interference [10].

Interacting percolation theory and stochastic geometry, we explore and develop the new parametrization to characterize the connectivity of the underlay secondary network. With the proposed parametrization, operating points corresponding to different transmit power allocation of SUs are obtained and represented by a Pareto contour in the phase space. Moreover, since the resulting operating end point of the underlay secondary network is located in the sub-critical region that will be defined later, percolation of the underlay secondary network can only be occurred across some time slots. This latency for the network to percolate (or latency-to-percolate) can be obtained, which represents the connectivity level of the network. Our framework leads to an unified understanding of the relationship among connectivity, interference, latency and other system parameters in the underlay secondary ad hoc CRN, facilitating designs and analysis of different network protocols.

The remainder of this paper is organized as follows. Section II presents the phase transition diagram, considering inter-system interference (between PUs and SUs) only. The effect of both inter-system and intra-system interference (i.e., self-cochannel interference among PUs or SUs) is addressed in Section III. Numerical results are provided along discussions. Section IV gives the conclusion.

II. Phase transition diagram

Consider a homogeneous network $\mathcal{G}(\lambda, r)$ with density of active nodes λ and transmission range r, two nodes are

regarded as connected if they are within r of each other. The resulting topology is generally described as a random geometric graph. The network $\mathcal{G}(\lambda, r)$ percolates, and a giant connected component exists when $\lambda r^2 > \lambda_c$, while the network breaks down in many isolated finite clusters when $\lambda r^2 < \lambda_c$, where $\lambda_c \approx 1.436$ is a constant. Phase transition of $\mathcal{G}(\lambda, r)$ occurs at $\lambda r^2 = \lambda_c$, and the region above (resp. below) the curve is called super-critical (resp. sub-critical) region.

A. Stand-alone secondary network

The spatial distribution of SUs is assumed to follow a homogeneous Poisson point process with density λ_{SU}, and we let $\Phi_{SU} = \{Y_i\}$ denote the locations of the SUs. The transmit power of an SU is denoted as P_{SU}. A pair of SUs is assumed to be connected if they are within radius r_{SU} of each other. r_{SU} satisfies

$$\mathbb{P}\left(\frac{G_{SU}P_{SU}r_{SU}^{-\alpha}}{N} \leq \eta_{SU}\right) = \epsilon_{SU}, \tag{1}$$

where G_{SU} is denoted as the channel power gain and is supposed to be exponential distributed with unit mean, α is the path loss exponent, N is the background noise power, η_{SU} is the SINR threshold of an SR, and an outage constraint is imposed on the SR with a maximum outage probability ϵ_{SU}. Note that here the transmission range is defined by an outage constraint. We assume that the stand-alone secondary network $\mathcal{G}(\lambda_{SU}, r_{SU})$ percolates (i.e., its corresponding operating point (λ_{SU}, r_{SU}) is within the super-critical region in the phase space). As will be needed in the following analysis, subset of SUs is always obtained by independent thinning of Φ_{SU} which is realized by the media access control scheme *slotted ALOHA*. The subset is denoted as $\Phi_{SU}(p) = \{Y_i : B_i(p) = 1\}$ with node density $p\lambda_{SU}$, where p is the media access probability of slotted ALOHA and $B_i(p)$ are i.i.d. Bernoulli random variables with parameter p.

B. Stand-alone primary network

The spatial distribution of PTs is also assumed to follow a homogeneous Poisson point process with density λ_{PT}, and the locations of the PTs are denoted as $\Phi_{PT} = \{X_i\}$. It represents the active transmitting set of PUs in a certain time slot with slotted ALOHA as the media access strategy. Each PT has transmit power P_{PT} and a dedicated PR, which is not a part of Φ_{PT}, located at a *fixed* distance r_{PT} away with an arbitrary direction. Note that the spatial distribution of PRs also forms a homogeneous Poisson point process with the same density correlated with that of PTs. Each PR has an SINR threshold η_{PR} and an outage constraint with a maximum outage probability ϵ_{PR}. We have

$$\mathbb{P}\left(\frac{G_{PT}P_{PT}r_{PT}^{-\alpha}}{N} \leq \eta_{PR}\right) \leq \epsilon_{PR}, \tag{2}$$

where G_{PT} is denoted as the channel power gain and is supposed to be exponential distributed with unit mean.

C. Underlay secondary network

Reminded that we only consider inter-system interference here, discussions on both inter-system and intra-system interference are addressed in Section III. When the secondary network $\mathcal{G}(\lambda_{SU}, r_{SU})$ is underlay with the primary network described above, we have the following two observations: (i) the interference from PTs results in reduction of the transmission range of an SU, i.e., r_{SU} reduces to $\widetilde{r}_{SU}$; and (ii) to avoid interference from SUs violating the outage constraint at a PR, only a proportion (subset) of SUs are allowed to transmit, i.e., λ_{SU} reduces to $\widetilde{\lambda}_{SU}$. In the phase space, the original operating point decreases in both dimensions and moves from (λ_{SU}, r_{SU}) to $(\widetilde{\lambda}_{SU}, \widetilde{r}_{SU})$. As shown in Fig. 1, when $(\widetilde{\lambda}_{SU}, \widetilde{r}_{SU})$ locates in the sub-critical region, phase transition of the secondary network occurs, and the resulting topology $\mathcal{G}(\widetilde{\lambda}_{SU}, \widetilde{r}_{SU})$ does not percolate. Above two results are described by the following lemmas.

Lemma 1. *The transmission range of an SU decreases form r_{SU} to $\widetilde{r}_{SU}$. That is, transmissions among SUs with distance greater than $\widetilde{r}_{SU}$ do not meet the outage constraint due to the interference from PTs.*

Proof: The outage constraint is maintained with $\widetilde{r}_{SU}$ satisfying

$$\mathbb{P}\left(\frac{G_{SU}P_{SU}\widetilde{r}_{SU}^{-\alpha}}{N + I_{PT}} \geq \eta_{SU}\right) = 1 - \epsilon_{SU}, \tag{3}$$

where $I_{PT} = \sum_{X_i \in \Phi_{PT}} G_{X_i} P_{PT} \|X_i\|^{-\alpha}$ is the interference from PTs to a typical (reference) SR located at the origin. By the stationary characteristic of homogeneous Poisson point process [11], the interference measured by the typical SR is representative of the interference seen by all other SRs. G_{X_i} and $\|X_i\|$ are respectively the channel power gain and the distance between the PT at X_i and the typical SR at the origin.

From [5], the moment generating function of I_{PT} is

$$\begin{aligned}
&\mathbb{E}[\exp(-sI_{PT})] \\
&= \exp\left\{-\lambda_{PT}\int_{\mathbb{R}^2} 1 - \mathbb{E}[\exp(-sGP_{PT}\|x\|^{-\alpha})]dx\right\} \\
&= \exp\left(-2\pi\lambda_{PT}\int_0^\infty \frac{u}{1 + \frac{u^\alpha}{sP_{PT}}}du\right) \\
&= \exp(-\lambda_{PT}P_{PT}^{2/\alpha}s^{2/\alpha}K_\alpha),
\end{aligned} \tag{4}$$

where $K_\alpha = \frac{2\pi^2}{\alpha \sin(2\pi/\alpha)}$. The left hand side of (3) can be evaluated as

$$\begin{aligned}
&\mathbb{P}\left[G_{SU} \geq \frac{\eta_{SU}}{P_{SU}\widetilde{r}_{SU}^{-\alpha}}(N + I_{PT})\right] \\
&= \exp\left(-\frac{\eta_{SU}}{P_{SU}\widetilde{r}_{SU}^{-\alpha}}N\right)\mathbb{E}\left[\exp\left(-\frac{\eta_{SU}}{P_{SU}\widetilde{r}_{SU}^{-\alpha}}I_{PT}\right)\right] \\
&= \exp\left(-\frac{\eta_{SU}}{P_{SU}\widetilde{r}_{SU}^{-\alpha}}N\right)\exp\left(-\lambda_{PT}\widetilde{r}_{SU}^2\left(\frac{\eta_{SU}P_{PT}}{P_{SU}}\right)^{\frac{2}{\alpha}}K_\alpha\right).
\end{aligned} \tag{5}$$

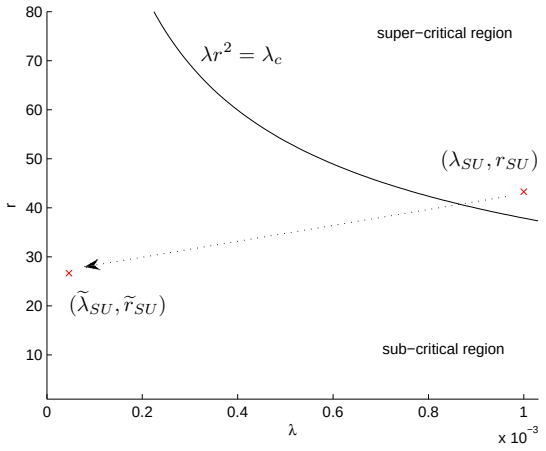

Fig. 1. Operating point moves from $(\lambda_{SU}, r_{SU}) = (1 \times 10^{-3}, 43.29)$ to $(\widetilde{\lambda}_{SU}, \widetilde{r}_{SU}) = (4.62 \times 10^{-5}, 26.68)$ due to inter-system interference

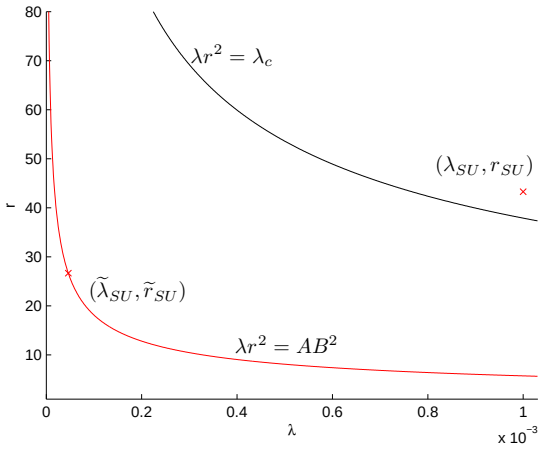

Fig. 2. Pareto contour with different transmit power of SUs

From (3) and (5), in the interference limited regime, we set $N = 0$ and have

$$\widetilde{r}_{SU} = \sqrt{\frac{-\ln(1-\epsilon_{SU})}{\lambda_{PT}(\frac{\eta_{SU}P_{PT}}{P_{SU}})^{\frac{2}{\alpha}}K_\alpha}}. \tag{6}$$

It can be seen that when λ_{PT} or P_{PT} increases, $\widetilde{r}_{SU}$ decreases. ■

Please note that the interference averaging in (3) is performed spatially. However, due to the randomness of the media access control protocol (slotted ALOHA) with small access probability, each node becomes active independent of other nodes and independent from time slot to time slot. Also, the channel gains are i.i.d. and are assumed to pick up different realizations in each time slot. The temporal correlation of the interference becomes small [12], and thus the link outage probability is also temporally averaged. The above analysis may be applied to other channel models with approximations on the outage probability [13, Theorem 1].

Lemma 2. *To avoid interference from SUs violating the outage constraint at a PR, the density of active SUs decreases from λ_{SU} to $\widetilde{\lambda}_{SU}$.*

Proof: The outage constraint at a PR is maintained when only a proportion $\widetilde{p}$ of SUs are allowed to transmit. This subset of SUs, denoted as $\Phi_{SU}(\widetilde{p})$ with density $\widetilde{\lambda}_{SU} = \widetilde{p}\lambda_{SU}$, is obtained by independent thinning of Φ_{SU} with probability $\widetilde{p}$ (slotted ALOHA). $\widetilde{p}$ (or $\widetilde{\lambda}_{SU}$) is derived by solving

$$\mathbb{P}\left(\frac{G_{PT}P_{PT}r_{PT}^{-\alpha}}{N + I_{SU}} \geq \eta_{PR}\right) = 1 - \epsilon_{PR}, \tag{7}$$

where $I_{SU} = \sum_{Y_i \in \Phi_{SU}(\widetilde{p})} G_{Y_i} P_{SU} \|Y_i\|^{-\alpha}$ is the interference from SUs to a typical PR located at the origin. The left hand side of (7) can be evaluated as

$$\begin{aligned}
&\mathbb{P}\left[G_{PT} \geq \frac{\eta_{PR}}{P_{PT}r_{PT}^{-\alpha}}(N + I_{SU})\right] \\
&= \exp\left(-\frac{\eta_{PR}}{P_{PT}r_{PT}^{-\alpha}}N\right)\mathbb{E}\left[\exp\left(-\frac{\eta_{PR}}{P_{PT}r_{PT}^{-\alpha}}I_{SU}\right)\right] \\
&= \exp\left(-\frac{\eta_{PR}}{P_{PT}r_{PT}^{-\alpha}}N\right)\exp\left(-\widetilde{\lambda}_{SU}r_{PT}^2\left(\frac{\eta_{PR}P_{SU}}{P_{PT}}\right)^{\frac{2}{\alpha}}K_\alpha\right).
\end{aligned} \tag{8}$$

From (7) and (8), in the interference limited regime, we have

$$\widetilde{\lambda}_{SU} = \frac{-\ln(1-\epsilon_{PR})}{r_{PT}^2(\frac{\eta_{PR}P_{SU}}{P_{PT}})^{\frac{2}{\alpha}}K_\alpha}. \tag{9}$$

It can be seen that when ϵ_{PR} decreases, $\widetilde{\lambda}_{SU}$ decreases. ■

Fig. 1 shows the above results. The system parameters are set as $N = 10^{-9}$, $\alpha = 4$, $\lambda_{SU} = 10^{-3}$, $P_{SU} = 0.1$, $\eta_{SU} = 3$, $\epsilon_{SU} = 0.1$, $\lambda_{PT} = 10^{-5}$, $P_{PT} = 0.3$, $r_{PT} = 15$, $\eta_{PR} = 3$, and $\epsilon_{PR} = 0.05$, which are used in all following numerical results.

D. Pareto contour

When the transmit power of SUs P_{SU} changes, $(\widetilde{\lambda}_{SU}(P_{SU}), \widetilde{r}_{SU}(P_{SU}))$ is recognized as a Pareto contour in the phase space. From (9) and (6), we respectively have

$$\widetilde{\lambda}_{SU}(P_{SU}) = \frac{-\ln(1-\epsilon_{PR})}{r_{PT}^2(\frac{\eta_{PR}}{P_{PT}})^{\frac{2}{\alpha}}K_\alpha}P_{SU}^{-\frac{2}{\alpha}} \triangleq AP_{SU}^{-\frac{2}{\alpha}}, \tag{10}$$

and

$$\widetilde{r}_{SU}(P_{SU}) = \sqrt{\frac{-\ln(1-\epsilon_{SU})}{\lambda_{PT}(\eta_{SU}P_{PT})^{\frac{2}{\alpha}}K_\alpha}}P_{SU}^{\frac{1}{\alpha}} \triangleq BP_{SU}^{\frac{1}{\alpha}}. \tag{11}$$

There exists a trade off between the density of active SUs and the transmission range of SUs. The Pareto contour is characterized by the equation

$$\widetilde{\lambda}_{SU}\widetilde{r}_{SU}^2 = AB^2. \tag{12}$$

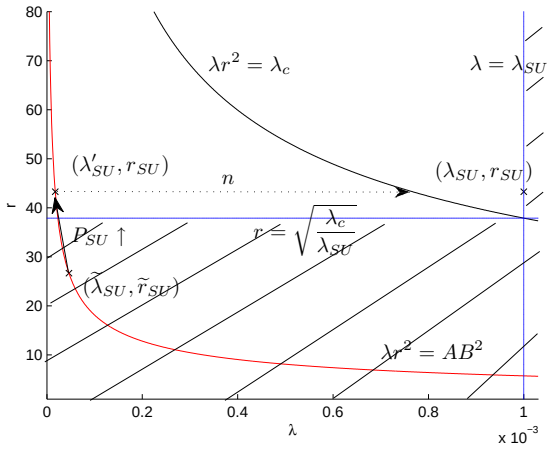

Fig. 3. The latency-to-percolate n at $(\lambda'_{SU}, r_{SU}) = (1.75 \times 10^{-5}, 43.29)$.

The resulting operating point of the underlay secondary network is able to move along the Pareto contour by changing the transmit power of SUs, which is shown in Fig. 2.

E. Latency-to-percolate

The operating point $(\widetilde{\lambda}_{SU}, \widetilde{r}_{SU})$ of the underlay secondary network is located in the sub-critical region; however, when observing the union of different realizations of the underlay secondary network over several time slots, the resulting *hyper* secondary network may percolate. In the *hyper* secondary network over n time slots, an SU is considered to be active when the SU is active at least once in the n time slots. As a result, suppose an SU in the underlay secondary network $\mathcal{G}(\widetilde{\lambda}_{SU}, \widetilde{r}_{SU})$ is active with probability $\widetilde{p} = \widetilde{\lambda}_{SU}/\lambda_{SU}$, the SU is active with probability $1-(1-\widetilde{p})^n$ in the corresponding *hyper* secondary network over n time slots, which percolates when $(1-(1-\widetilde{p})^n)\lambda_{SU}\widetilde{r}_{SU}^2 \geq \lambda_c$. The latency-to-percolate is defined as the total time slots n such that

$$n = \frac{\ln\left(1-\frac{\lambda_c}{\lambda_{SU}\widetilde{r}_{SU}^2}\right)}{\ln(1-\widetilde{p})} = \frac{\ln\left(1-\widetilde{p}\frac{\lambda_c}{AB^2}\right)}{\ln(1-\widetilde{p})}. \quad (13)$$

Since $\widetilde{\lambda}_{SU} \leq \lambda_{SU}$, we observe that $\widetilde{p} \leq 1$ in (13). Also, since $\lambda_{SU}\widetilde{r}_{SU}^2 \geq (1-(1-\widetilde{p})^n)\lambda_{SU}\widetilde{r}_{SU}^2 \geq \lambda_c$, we have $\widetilde{r}_{SU} \geq \sqrt{\lambda_c/\lambda_{SU}}$ corresponding to $\widetilde{p} \leq AB^2/\lambda_c$ in (13). Thus, as indicated in Fig. 3, not every resulting operating point of the underlay secondary network can be defined a percolated *hyper* secondary network. There exists the minimum transmission range and the maximum density of active SUs.

On the other hand, the operating point is able to move along the Pareto contour by increasing the transmit power of SUs. As shown in Fig. 3, for example, the operating point $(\widetilde{\lambda}_{SU}, \widetilde{r}_{SU})$ moves to (λ'_{SU}, r_{SU}) indicated by the label $P_{SU} \uparrow$ (power increasing). With the increasing power, the transmission range changes back to r_{SU}, while the density of active SUs decreases from $\widetilde{\lambda}_{SU}$ to $\lambda'_{SU} = \frac{AB^2}{r_{SU}^2}$. The corresponding latency-to-percolate can be derived as $n = \ln\left(1-\frac{\lambda_c}{\lambda_{SU}r_{SU}^2}\right)/\ln\left(1-\frac{AB^2}{\lambda_{SU}r_{SU}^2}\right)$. Note that the latency-to-percolation of (λ'_{SU}, r_{SU}) is different from the average media access delay of an SU, which is $\frac{1}{p'} = \frac{\lambda_{SU}}{\lambda'_{SU}} = \frac{\lambda_{SU}r_{SU}^2}{AB^2}$.

When $\widetilde{p}$ decreases (or P_{SU} increases), the latency-to-percolate decreases and the limit exists,

$$\lim_{\widetilde{p}\to 0} n = \lim_{\widetilde{p}\to 0} \frac{\ln\left(1-\widetilde{p}\frac{\lambda_c}{AB^2}\right)}{\ln(1-\widetilde{p})} = \frac{\lambda_c}{AB^2}, \quad (14)$$

which is the lower bound of the latency-to-percolate of any operating point in the Pareto contour.

F. Avoidance region

If an SU is in the vicinity of a PR, deactivation of the SU (instead of following the slotted ALOHA scheme with certain access probability) may increase the overall allowed density of active SUs maintaining the same outage constraints of PRs. With the sensing and cognitive capability of CR, an SU is deactivated when it is located within radius ρ of any PR; in other words, each PR has an SU-avoidance region with radius ρ. The probability of an SU located in $\mathcal{B}(PR;\rho)$ is $1-\exp(-\lambda_{PT}\pi\rho^2)$, where the notation $\mathcal{B}(x;r)$ represents a circle of radius r centered at x. The interference from SUs to a typical PR located at the origin becomes

$$I_{SU}^{\rho} = \sum_{Y_i \in \Phi_{SU}(\widetilde{p}^{\rho})\setminus\mathcal{B}(0;\rho)} G_{Y_i} P_{SU} \|Y_i\|^{-\alpha} \mathbf{1}_{Y_i \notin \mathcal{B}(PR;\rho)}, \quad (15)$$

where $\mathbf{1}_{Y_i\notin\mathcal{B}(PR;\rho)}$ is the indicator function which shows that any SU located in the avoidance region of any PR is not added to the interference. Please note that (15) presumes independent thinning of each SU outside $\mathcal{B}(0;\rho)$ with probability $\exp(-\lambda_{PT}\pi\rho^2)$. The real interference statistics is only approximated since the event that an SU is located in an avoidance region is correlated with a nearby SU being within the same avoidance region. The approximation is reasonable as the avoidance region is small.

The moment generating function of I_{SU}^{ρ} is

$$\mathbb{E}[\exp(-sI_{SU}^{\rho})] = \exp\left(-2\pi\widetilde{\lambda}_{SU}^{\rho}\exp(-\lambda_{PT}\pi\rho^2)\int_{\rho}^{\infty}\frac{u}{1+\frac{u^{\alpha}}{sP_{SU}}}du\right) \quad (16)$$

Substituting $s = \frac{\eta_{PR}}{P_{PT}r_{PT}^{-\alpha}}$ and $\alpha = 4$ in (16), we have the closed-form expression

$$\mathbb{E}\left[\exp\left(-\frac{\eta_{PR}}{P_{PT}r_{PT}^{-\alpha}}I_{SU}^{\rho}\right)\right] = \exp\left\{-\widetilde{\lambda}_{SU}^{\rho}\exp(-\lambda_{PT}\pi\rho^2)\pi r_{PT}^2\left(\frac{\eta_{PR}P_{SU}}{P_{PT}}\right)^{\frac{1}{2}} \times\left[\frac{\pi}{2}-\tan^{-1}\left(\sqrt{\frac{P_{PT}}{\eta_{PR}P_{SU}}}\frac{\rho^2}{r_{PT}^2}\right)\right]\right\}. \quad (17)$$

We compare the overall allowed density of active SUs with avoidance region to that without avoidance region, i.e., $\rho = 0$.

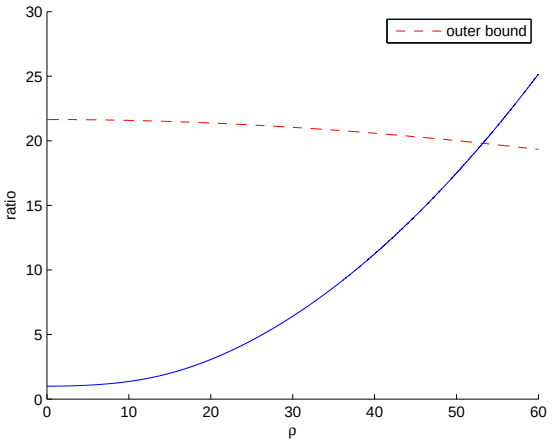

Fig. 4. The ratio of the overall allowed SU density with avoidance region to that without avoidance region v.s. ρ.

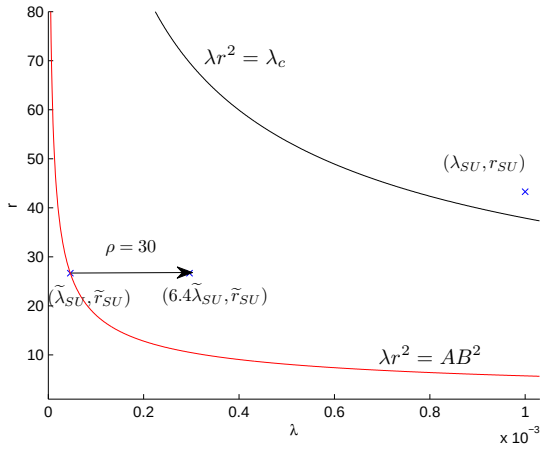

Fig. 5. Operating point changes after insertion of avoidance region

The ratio is

$$\frac{\widetilde{\lambda}_{SU}^{\rho}\exp(-\lambda_{PT}\pi\rho^2)}{\widetilde{\lambda}_{SU}} = \frac{\pi/2}{\pi/2 - \tan^{-1}(\sqrt{\frac{P_{PT}}{\eta_{PR}P_{SU}}}\frac{\rho^2}{r_{PT}^2})} \geq 1, \tag{18}$$

where $\widetilde{\lambda}_{SU} = \widetilde{\lambda}_{SU}^{0}$, and the term $\exp(-\lambda_{PT}\pi\rho^2)$ in the numerator indicates the probability of an SU located outside avoidance regions. Obviously, $\lambda_{SU}\exp(-\lambda_{PT}\pi\rho^2)/\widetilde{\lambda}_{SU}$ is an outer bound of (18) which decreases as ρ increases.

Fig. 4 shows the ratio in (18) which is a good approximation of the real increment when ρ is small. When the density of SUs λ_{SU} is large enough, with the notion of avoidance region, the overall allowed density of active SUs increases tremendously. Fig. 5 shows the result with $\rho = 30$. Intuitively, by choosing a suitable radius ρ, we can prevent possible outage reception at a PR caused by the interference from a single dominant SU.

Remark. *Rigorously speaking, with the avoidance region, the resulting spatial distribution of SUs is no longer a homogeneous Poisson point process. Moreover, when the radius ρ of the avoidance region increases and achieves the equation,*

$$\lambda_{PT} = \frac{\lambda_c/4}{\rho^2 - \widetilde{r}_{SU}^2/4}, \tag{19}$$

the avoidance regions percolate and overlap with each other with "width" $\widetilde{r}_{SU}$ corresponding to the transmission range of SUs [14]. It is the sufficient condition for the operating point of the underlay secondary network to be located at the sub-critical region, served as another possible dimension of parametrization.

III. Inter-system and intra-system interference

In previous section, we only account for inter-system interference; however, intra-system interference also plays an important role in network performance.

A. Intra-system interference only

First, we consider intra-system interference among SUs only, we have

$$\begin{aligned}
&\mathbb{P}\left[G_{SU} \geq \frac{\eta_{SU}}{P_{SU}\widetilde{r}_{SU}^{-\alpha}}(N + I_{SU})\right] \\
&= \exp\left(-\frac{\eta_{SU}}{P_{SU}\widetilde{r}_{SU}^{-\alpha}}N\right)\mathbb{E}\left[\exp\left(-\frac{\eta_{SU}}{P_{SU}\widetilde{r}_{SU}^{-\alpha}}I_{SU}\right)\right] \\
&= \exp\left(-\frac{\eta_{SU}}{P_{SU}\widetilde{r}_{SU}^{-\alpha}}N\right)\exp(-\widetilde{\lambda}_{SU}\widetilde{r}_{SU}^2\eta_{SU}^{\frac{2}{\alpha}}K_\alpha).
\end{aligned} \tag{20}$$

In the interference limited regime, having an outage constraint ϵ_{SU} on SR, we arrive at the Pareto contour

$$\widetilde{\lambda}_{SU}\widetilde{r}_{SU}^2 = \frac{-\ln(1-\epsilon_{SU})}{K_\alpha\eta_{SU}^{\frac{2}{\alpha}}} \triangleq C, \tag{21}$$

which is depicted in Fig. 6. It characterizes the effect of self co-channel interference that also leads to phase transition of the secondary network. The analysis of latency-to-percolate follows previous discussions.

B. Inter-system and intra-system interference

When we account for both inter-system and intra-system interference, (8) becomes

$$\begin{aligned}
&\mathbb{P}\left[G_{PT} \geq \frac{\eta_{PR}}{P_{PT}r_{PT}^{-\alpha}}(N + I_{SU} + I_{PT})\right] \\
&= \exp\left(-\frac{\eta_{PR}}{P_{PT}r_{PT}^{-\alpha}}N\right)\mathbb{E}\left[\exp\left(-\frac{\eta_{PR}}{P_{PT}r_{PT}^{-\alpha}}I_{SU}\right)\right] \\
&\quad\times\mathbb{E}\left[\exp\left(-\frac{\eta_{PR}}{P_{PT}r_{PT}^{-\alpha}}I_{PT}\right)\right] \\
&= \exp\left(-\frac{\eta_{PR}}{P_{PT}r_{PT}^{-\alpha}}N\right)\exp\left(-\widetilde{\lambda}_{SU}r_{PT}^2\left(\frac{\eta_{PR}P_{SU}}{P_{PT}}\right)^{\frac{2}{\alpha}}K_\alpha\right) \\
&\quad\times\exp(-\lambda_{PT}r_{PT}^2\eta_{PR}^{\frac{2}{\alpha}}K_\alpha).
\end{aligned} \tag{22}$$

Since we have an outage constraint ϵ_{PR} on PR, in the interference limited regime, the maximum density of active

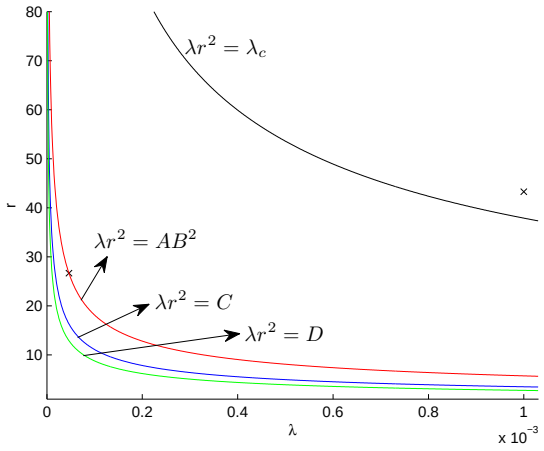

Fig. 6. Pareto contour with inter-system interference $\lambda r^2 = AB^2$, intra-system interference $\lambda r^2 = C$, inter-system and intra-system interference $\lambda r^2 = D$.

SUs is

$$\widetilde{\lambda}_{SU} = \left(\frac{-\ln(1-\epsilon_{PR})}{r_{PT}^2 \eta_{PR}^{\frac{2}{\alpha}} K_\alpha} - \lambda_{PT} \right) \left(\frac{P_{PT}}{P_{SU}} \right)^{\frac{2}{\alpha}} \triangleq A' P_{SU}^{-\frac{2}{\alpha}}. \quad (23)$$

In addition, (5) becomes

$$\begin{aligned} &\mathbb{P}\left[G_{SU} \geq \frac{\eta_{SU}}{P_{SU} \widetilde{r}_{SU}^{-\alpha}} (N + I_{PT} + I_{SU}) \right] \\ &= \exp\left(-\frac{\eta_{SU}}{P_{SU} \widetilde{r}_{SU}^{-\alpha}} N \right) \mathbb{E}\left[\exp\left(-\frac{\eta_{SU}}{P_{SU} \widetilde{r}_{SU}^{-\alpha}} I_{PT} \right) \right] \\ &\quad \times \mathbb{E}\left[\exp\left(-\frac{\eta_{SU}}{P_{SU} \widetilde{r}_{SU}^{-\alpha}} I_{SU} \right) \right] \\ &= \exp\left(-\frac{\eta_{SU}}{P_{SU} \widetilde{r}_{SU}^{-\alpha}} N \right) \exp\left(-\lambda_{PT} \widetilde{r}_{SU}^2 \left(\frac{\eta_{SU} P_{PT}}{P_{SU}} \right)^{\frac{2}{\alpha}} K_\alpha \right) \\ &\quad \times \exp(-\widetilde{\lambda}_{SU} \widetilde{r}_{SU}^2 \eta_{SU}^{\frac{2}{\alpha}} K_\alpha). \end{aligned} \quad (24)$$

Since we have an outage constraint ϵ_{SU} on SR, in the interference limited regime, the transmission range is

$$\widetilde{r}_{SU} = \sqrt{ \frac{-\ln(1-\epsilon_{SU})}{K_\alpha \eta_{SU}^{\frac{2}{\alpha}} (\lambda_{PT} (\frac{P_{PT}}{P_{SU}})^{\frac{2}{\alpha}} + A' P_{SU}^{-\frac{2}{\alpha}})} } \triangleq B' P_{SU}^{\frac{1}{\alpha}}. \quad (25)$$

Combining (23) and (25), we have

$$\widetilde{\lambda}_{SU} \widetilde{r}_{SU}^2 = A' B'^2 \triangleq D. \quad (26)$$

The above result is shown in Fig. 6. We observe that both inter-system and intra-system interference lead to phase transition of the secondary network, and their joint effect is reflected by the bottom-most contour in the figure. Latency-to-percolate can be obtained as discussed previously, which indicates overall connectivity degradation due to the interference. Design of QoS-aware service in the underlay secondary ad hoc CRN may be guided by the analysis.

IV. Conclusion

While coexisting with a primary ad hoc network, in consideration of avoiding excess interference to PRs and being interfered by PTs, topology of the underlay secondary network is changed. Both the density of active SUs and the transmission range of an SU decreases leading to additional media access delay and link reliability reduction respectively. Performance of end-to-end packet transmissions in the underlay secondary network is thus degraded.

To clarify the complicated relationship among connectivity, interference, latency and other system parameters and to facilitate further analysis of performance of end-to-end packet transmissions, we provide a novel parametrization of the secondary network regarded as an operating point in the phase space. The underlay secondary network undergoes a phase transition and latency-to-percolate is induced. Different power allocation of SUs is described by a Pareto contour. With cognitive capability, analytic result shows that performance is improved with the notion of avoidance region. Further study and analysis of upper layer protocols and mechanisms may be built on the proposed framework.

References

[1] O. Dousse, F. Baccelli, and P. Thiran, "Impact of interferences on connectivity in ad hoc networks," *IEEE/ACM Trans. Netw.*, vol. 13, no. 2, pp. 425–436, Apr. 2005.

[2] M. Franceschetti and R. Meester, *Random Networks for Communication: From Statistical Physics to Information Systems*. Cambridge University Press, 2008.

[3] S. Weber, X. Yang, J. Andrews, and G. de Veciana, "Transmission capacity of wireless ad hoc networks with outage constraints," *IEEE Trans. Inf. Theory*, vol. 51, no. 12, pp. 4091–4102, Dec. 2005.

[4] S. Weber, J. Andrews, and N. Jindal, "The effect of fading, channel inversion, and threshold scheduling on ad hoc networks," *IEEE Trans. Inf. Theory*, vol. 53, no. 11, pp. 4127–4149, Nov. 2007.

[5] F. Baccelli, B. Blaszczyszyn, and P. Muhlethaler, "An aloha protocol for multihop mobile wireless networks," *IEEE Trans. Inf. Theory*, vol. 52, no. 2, pp. 421–436, Feb. 2006.

[6] V. Chandrasekhar and J. Andrews, "Uplink capacity and interference avoidance for two-tier femtocell networks," *IEEE Trans. Wireless Commun.*, vol. 8, no. 7, pp. 3498–3509, Jul. 2009.

[7] S.-M. Cheng, W. C. Ao, and K.-C. Chen, "Downlink capacity of two-tier cognitive femto networks," in *Proc. IEEE PIMRC 2010*, Sept. 2010, accepted for publication.

[8] K. Huang, V. Lau, and Y. Chen, "Spectrum sharing between cellular and mobile ad hoc networks: transmission-capacity trade-off," *IEEE J. Sel. Areas Commun.*, vol. 27, no. 7, pp. 1256–1267, Sept. 2009.

[9] C. Yin, L. Gao, T. Liu, and S. Cui, "Transmission capacities for overlaid wireless ad hoc networks with outage constraints," in *Proc. IEEE ICC '09*, Jun. 2009, pp. 1–5.

[10] W. Ren, Q. Zhao, and A. Swami, "Connectivity of heterogeneous wireless networks," *IEEE Trans. Inf. Theory*, 2009, submitted for publication. [Online]. Available: http://arxiv.org/abs/0903.1684

[11] J. Kingman, *Poisson Processes*. Oxford University Press, 1993.

[12] R. Ganti and M. Haenggi, "Spatial and temporal correlation of the interference in aloha ad hoc networks," *IEEE Commun. Lett.*, vol. 13, no. 9, pp. 631 –633, Sept. 2009.

[13] A. Hunter, J. Andrews, and S. Weber, "Transmission capacity of ad hoc networks with spatial diversity," *IEEE Trans. Wireless Commun.*, vol. 7, no. 12, pp. 5058 –5071, Dec. 2008.

[14] W. C. Ao, S.-M. Cheng, and K.-C. Chen, "Power and interference control with relaying in cooperative cognitive radio networks," in *Proc. IEEE ICC'10 Workshop CRISP*, May 2010.